Design and Development of a Low-cost Integrated Dosimeter for External Beam Dosimetry in Radiation Oncology

Tim Chant, Prabhakar Ramachandran

Department of Radiation Oncology, Therapeutic Physics, Cancer Services, Princess Alexandra Hospital, Woolloongabba, Queensland, Australia

Abstract

Radiation dosimeters play a crucial role in radiation oncology by accurately measuring radiation dose, ensuring precise and safe radiation therapy. This study presents the design and development of a low-cost printed circuit board (PCB) dosimeter and an integrated electrometer with sensitivity optimized for dose rates intended for use in megavoltage radiation therapy. The PCB dosimeter was designed in KiCad, and it uses a low-cost S5MC-13F general-purpose 1 kV 5A power diode as a radiation detector. The dosimeter is calibrated against a known dose derived from an ionization chamber and tested for dose linearity, dose rate dependence, field size dependence, and detector orientation dependence. The observed average dose differences between the delivered and measured doses for most measurements were found to be < 1.1%; the dose rate linearity between 100 MU/min and 1400 MU/min was found to be within 1.3%. This low-cost architecture could successfully be adapted further for a scalable, cost-effective dosimetry solution through firmware or circuit design.

Keywords: Diodes, dosimetry, operational amplifiers, radiation detectors, radiation oncology

INTRODUCTION

Radiation oncology is a key component of cancer management, with 50% of all cancer patients estimated to benefit from radiotherapy.[1] At the core of this treatment, precise dosimetry is imperative for guaranteeing the accurate application of therapeutic radiation doses while safeguarding adjacent healthy tissues.[2] Clinical radiotherapy medical physicists play a crucial role in overseeing the meticulous administration of prescribed dose distributions to patients. The use of ionization chambers, calibrated against primary standards,[3,4] ensures the precise measurement of absolute dose delivered to the tumor volume. Complementing this approach, thermoluminescent dosimeters,[5] metal–oxide–semiconductor field-effect transistors,[6] semiconductor detectors such as diodes,[7] and diamond detectors[8] have been used. In addition, optically stimulated luminescence dosimeters,[9] calorimeters,[10] and alanine-based dosimeters[11] contribute to the quantification of the dose administered to cancer patients. Notably, relative or spatial dosimetry is carried out through the deployment of arrays of ionization chambers/diodes,[12] films,[13] gel dosimeters,[14] and scintillation detectors.[15] A combination of absolute and relative dosimetry measurements representing dose delivery conditions guarantees both accuracy and safety in the planning and delivery of radiation therapy. As technology advances, radiation detectors continue to evolve, promising even greater precision and improved outcomes for patients undergoing radiation therapy.

The inclusion of affordable radiation detectors is crucial to enhance the accessibility of radiation therapy, particularly in settings with limited resources.[16] This strategic integration addresses a pressing need by making radiation treatment more attainable for a wider patient demographic, which is especially significant in regions with restricted health-care infrastructure. This also allows for more frequent and comprehensive dosimetry quality assurance practices, thereby improving treatment quality and safety.[17] In this study, we propose a low-cost radiation dosimeter that not only provides a solution for routine absolute dosimetry but also offers versatility as a stand-alone device or as a plug-and-play component within existing systems.

Address for correspondence: Prof. Prabhakar Ramachandran,
Therapeutic Physics, Cancer Services, Princess Alexandra Hospital,
Woolloongabba 4102, Queensland, Australia.
E-mail: prabhakar.ramachandran@health.qld.gov.au

How to cite this article: Chant T, Ramachandran P. Design and development of a low-cost integrated dosimeter for external beam dosimetry in radiation oncology. J Med Phys 2023;48:392-7.

METHODS

To achieve the goal of creating an affordable dosimeter, a design was crafted that exclusively utilizes readily accessible consumer-grade components. The components include the popular Espressif ESP8266 low-cost microcontroller with an inbuilt 10-bit analog-to-digital converter (ADC), a general-purpose power diode as the radiation-sensitive detector, and a charge-sensitive amplifier (CSA) front-end utilizing a combination of precision operational amplifiers, analog switches, and precision film capacitors. This device was constructed and subsequently tested and characterized on an Elekta linear accelerator (linac) using 6 MV and 6 MV flattening filter-free (FFF) X-rays. The diode selected as the radiation-sensitive detector was a S5MC-13F general-purpose 1 kV 5A power diode. This diode was chosen for its low cost ($0.50), large silicon die providing good sensitivity, symmetrical lead frame, and standard surface mount SMC package.

The PCB was designed in KiCad as a two-layer design that is easily manufacturable by PCB fabricators at minimal cost, with the limiting factor being the length of the PCB. Fifteen of those prototype PCBs [Figure 1a and b] were manufactured for $50, and the total material cost was approximately $30. The layout uses SOT-23-, 1206-, and 0603-sized components for a trade-off between miniaturization of the dosimeter and ease of assembly. An additional ADS1115 16-bit ADC was proposed to be used in the final implementation but was removed due to small improvement in useful accuracy, noise-free resolution, increased software complexity, and feedback that a very-thin shrink small-outline package (VSSOP) size would limit ease of assembly.

The CSA converts the small charge (≈400 nC/Gy) generated by the detector diode into a voltage that is large enough for the microcontroller's ADC to digitize with sufficient resolution. The CSA architecture has the detector diode operating without a bias voltage in photovoltaic mode to reduce design complexity at the cost of sensitivity. The radiation dose rates in radiation therapy treatment units are generally much higher compared to what is typically measured by environmental survey and personal dosimeters, thus sensitivity and subsequent gain requirements are several orders of magnitude lower, allowing for a greater flexibility of design choices.

The detector diode is placed directly across the inverting and noninverting inputs of a modern precision low input bias/offset op-amp (MCP6491T-E/OT), which drives the output to cancel out any voltage generated by the diode. The output drive achieves this through a feedback loop consisting of an integration capacitor; as a result, the op-amp output voltage is directly correlated with the charge generated by the diode. The value of the integration capacitor (C_f) determines the charge-to-voltage gain as shown in equation (1); a smaller capacitance results in higher gain. The input charge to be integrated is q_{in}, $N_{D,w,Q}$ is the diode calibration factor for absorbed dose to water in a beam of quality Q, D_w is the absorbed dose to water as measured by the diode, v_{out} is the front-end output voltage signal digitized by the microcontroller unit (MCU) ADC. For a v_{out} of 1V, the dose measured by the low-cost detector with a 22 nF capacitor will be approximately 0.063 Gy (equation [3]).

$$v_{out} = -\frac{q_{in}}{C_f} \tag{1}$$

$$v_{out} = -\frac{D_w \times N_{D,w,Q}}{C_f} \tag{2}$$

$$D_w = -\frac{v_{out} \times C_f}{N_{D,w,Q}} = -\frac{(1.0\ V \times 22\ nF)}{-345.44\ nC/Gy} \approx 0.063\ Gy \tag{3}$$

This CSA design integrates the total charge generated by the diode, which will saturate when the op-amp output reaches 3.3 V. This limitation is avoided by implementing a charge reset mechanism with a TS5A4594DBVR analog switch across the
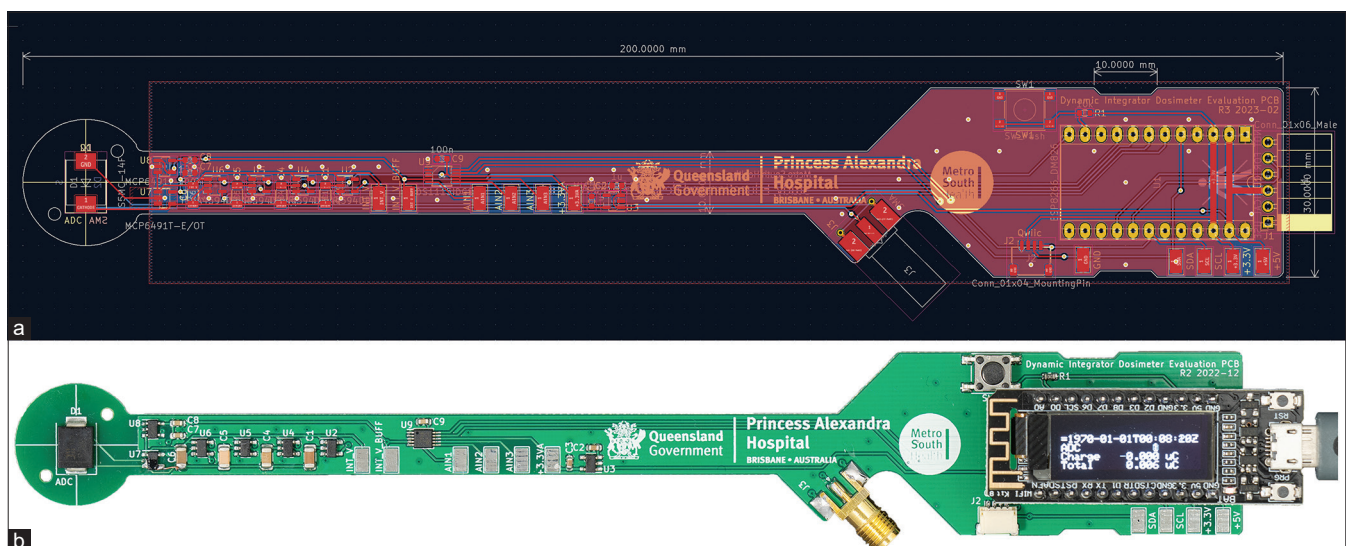

Figure 1: (a) Schematic diagram of the printed circuit board. (b) A single diode dosimeter

feedback capacitor, which discharges the integration capacitor for 100 μs through the approximately 8 Ω on-state resistance of the analog switch. Figure 2 illustrates the green trace, depicting the CSA output voltage over multiple integrations, ramping up and resetting once per second during the end of an exposure in the linac. It shows that the integration signal has a positive ramp, despite the negative gain of the front-end, due to the reversed diode polarity giving a negative k_{Gy} constant. The yellow trace shows the reset signal for the analog switch.

For higher dynamic range and usefulness across different applications, the CSA circuit also implements multiple selectable integration capacitors through multiple analog switches, allowing dynamic changes to the gain without the need to physically attach a new capacitor. It should be noted that there is a trade-off between the number of selectable integration capacitors and the leakage and injected current each analog switch introduces. The output of this CSA with selectable gain is then fed into another op-amp to buffer the signal and prevent the resistive divider on the microcontroller ADC from loading down the integration signal. The schematic of this circuit is shown in Figure 3.

The design also implements several development and verification features including test points to measure key system voltages and signals with an oscilloscope, a Qwiic/STEMMA I²C connector, UART header, and a second detector diode on the back side of the PCB connected to an SMA connector. These features can be used to verify the performance of the front-end and MCU ADC against a commercial electrometer.

The ESP8266 is programmed in C++ through the Arduino IDE due to the large number of existing libraries and the simplicity of re-flashing firmware over USB. The main task of this firmware is to acquire the voltage of the integrator's output using the 10-bit ADC of the ESP8266 and then reset the accumulated charge if it is above a predetermined voltage threshold or a time threshold has elapsed. This firmware has multiple methods for outputting dose data, the simplest of which displays the data in Gray on the built-in OLED display. The raw ADC time series data can also be transmitted through the ESP8266's serial interface along with a timestamp acquired on boot from an Internet NTP server over Wi-Fi; this output method was used for all evaluation tests and provides the most data without any limitations. The total dose and a small buffer of time series data are also available through a HTTP GET request over the MCU's Wi-Fi. However, due to limitations of the low-cost single-core MCU, the separate mode writing to the OLED display or handling Wi-Fi takes time, affecting the accuracy of the dose rate measurement window (though total accumulated dose is not affected). Therefore, the different modes are handled separately, but this allows for high-resolution (100 samples/sec) acquisition to be achieved in serial data-only mode. Nevertheless, this approach allows straightforward adjustment of the detector calibration factor.

The low-cost dosimeter was calibrated against a known dose derived from measurements using a 0.6 cm³ ionization chamber with a calibration traceable to the ARPANSA's primary standard dosimetry laboratory. A three-dimensional (3D) printed 2 cm water equivalent thick phantom was designed to house the low-cost dosimeter, with the diode effective point of measurement placed into the central position. The phantom was printed in PLA and then coated in viscous, fast-setting 2-part epoxy to make it watertight then filled with 2-part deep cast art epoxy to fill the entire shell. The Solid Water ® HE slabs with a dimension of 30 cm × 30 cm and various thicknesses were used for all other phantom materials. Figure 4 illustrates the 3D-printed slabs positioned between the solid water HE slabs, with the detector situated 10 cm from the phantom's surface.

Dose linearity was determined at specific doses of 10 cGy, 25 cGy, 50 cGy, 75 cGy, 100 cGy, 200 cGy, 500 cGy, and 1000 cGy. The dose rate dependence of the dosimeter was performed at 100 MU/min, 400 MU/min, 700 MU/min, and 1400 MU/min. The performance of the low-cost dosimeter at various detector orientations, such as the top-up, bottom-up, anode-up, and cathode-up, was also performed. Measurements in the anode-up and cathode-up positions were performed at gantry angles of 90° and 270°, respectively. In addition, the field size dependency was also performed for 3 cm × 3 cm, 5 cm × 5 cm, 7 cm × 7 cm, 8 cm × 8 cm, 10 cm × 10 cm, 12 cm × 12 cm, 15 cm × 15 cm, 18 cm × 18 cm, 20 cm × 20 cm and 25 cm × 25 cm. For all measurements, the dosimeter was placed at a 10 cm depth and 90 cm source to surface distance (SSD).

RESULTS

Figure 5 is a cumulative dose plot demonstrating gain linearity and dose rate dependence for multiple exposures for 6 MV and 6 MV FFF beams. The linac output (1 cGy/MU) is defined at a depth of 10 cm and a SSD of 90 cm for a field size of 10 cm × 10 cm.

Table 1 illustrates the agreement between the measured and delivered doses for 6 MV beams with flattening filter using a 100 nF integration capacitor, for a 10 cm ×10 cm field size at 10 cm depth. The maximum observed dose differences between the delivered and measured doses were found to be <1.3%.

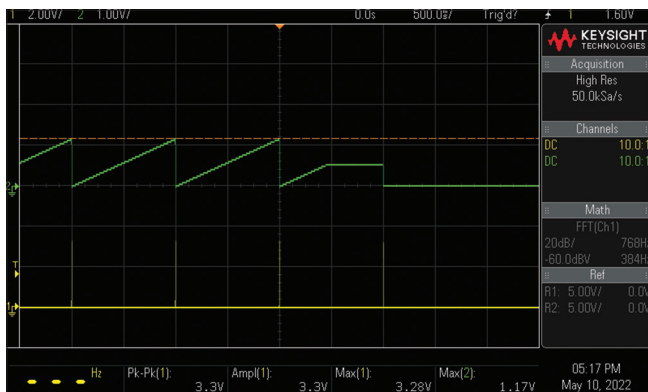**Figure 2:** Oscilloscope screen capture showing charge-sensitive amplifier ramp waveform at the end of a linac exposure
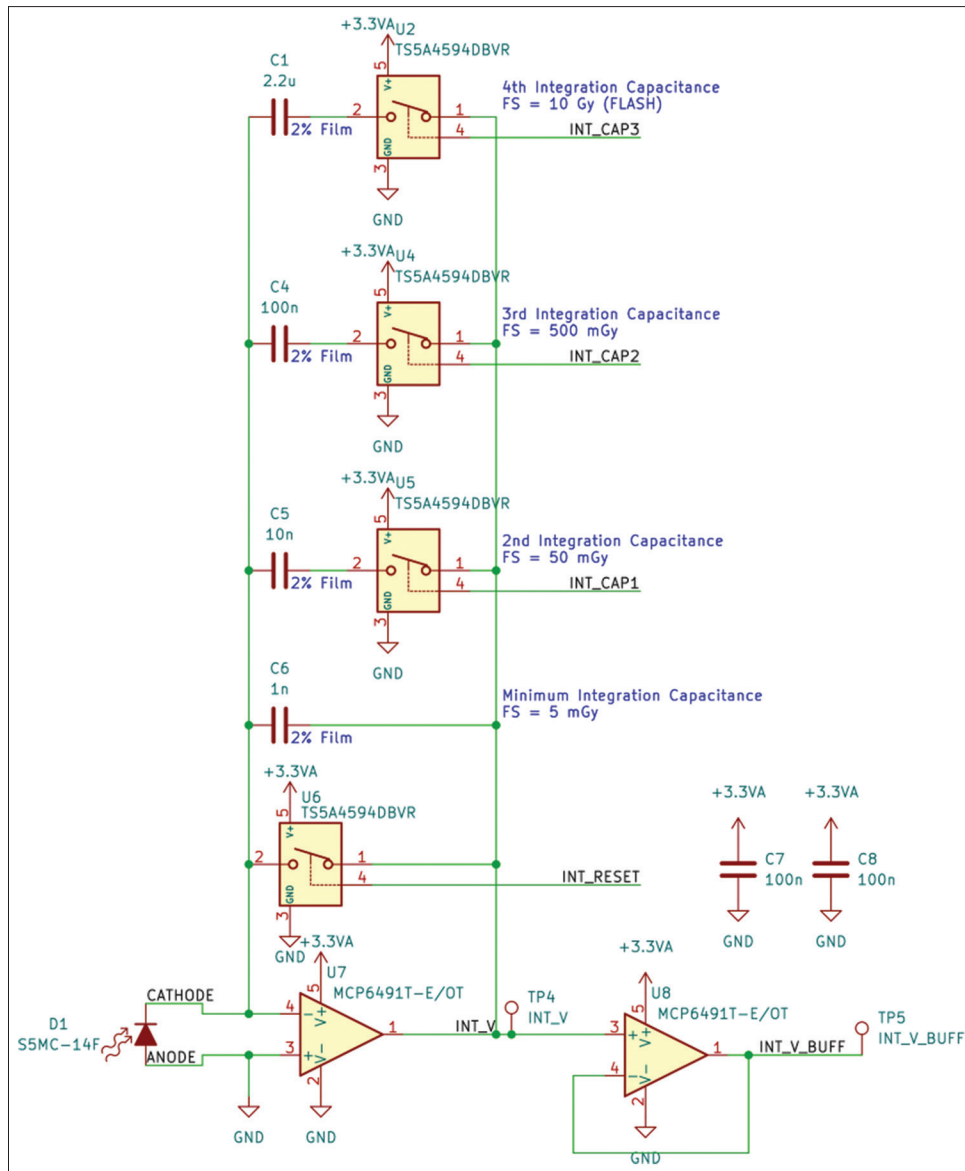
Figure 3: Schematic diagram of circuit indicating the diode, op-amps, switches, and integration capacitors

The measured doses for 100 MU at 100 MU/min (6 MV), 400 MU/min (6 MV), 700 MU/min (6 MV FFF), and 1300 MU/min (6 MV FFF) were found to be 0.64%, 1.07%, 0.93%, and 1.3%, respectively. The output factors measured from 3 cm ×3 cm to 25 cm ×25 cm agreed within 1.0% of the ion chamber measured reference values. Table 2 illustrates the sensitivity of the diode when placed in different orientations to the incident beam. The anode-up orientation showed a maximum error of up to 11%. For dosimetry purposes, the detector is recommended to be in either a top-up or a bottom-up orientation.

Figure 6 shows the gain linearity for four different gain settings (low, medium, high and highest) at multiple exposures between 10 cGy and 1000 cGy. The linear curve at the bottom of the figure highlights the error bars for low gain. For medium, high, and highest gains, the error range is so small that is closer to the plotted points.

DISCUSSION AND CONCLUSION

The low-cost radiation dosimeter, tested for 6 MV X-rays, has demonstrated good performance across various conditions. The observed variation of 0.64%, 1.07%, 0.93%, and 1.3% for 100 MU/min (6 MV), 400 MU/min (6 MV), 700 MU/min (6 MV FFF), and 1300 MU/min, respectively, was based on the detector calibration at 400 MU/min performed several weeks prior to these measurements. The variation highlights the output fluctuations on the day of measurements. The detector performed well in the top-up (to within 0.4%) and bottom-up (to within 0.8%) orientations, but in the anode-up and cathode-up orientations, it exhibited dose measurements beyond the tolerance of 2%. The cathode-up and anode-up positions arise when the diode's top surface is parallel to the beam's central axis, which takes place when the gantry is at 90° or 270°, necessitating angular corrections during dose
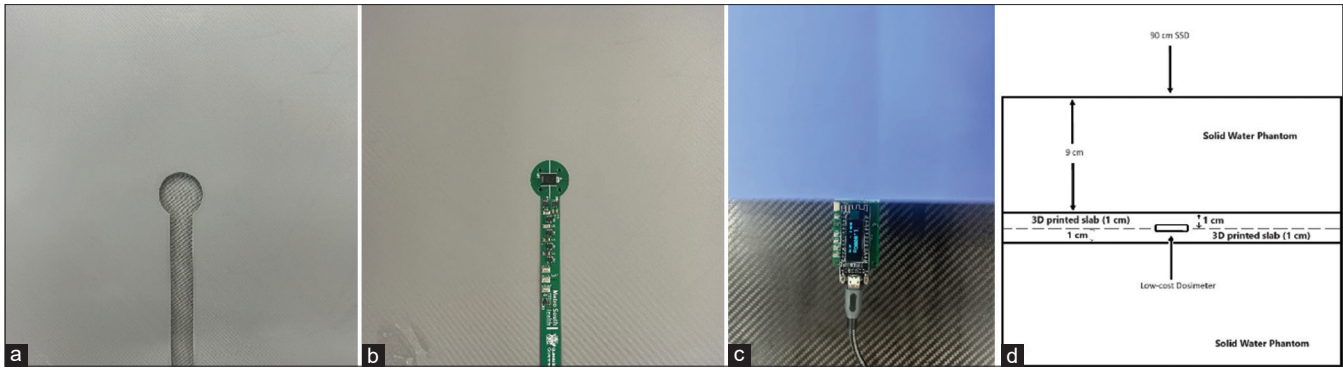
Figure 4: (a) Three-dimensional (3D)-printed slab with a cavity designed for housing the dosimeter, (b) dosimeter positioned within the cavity of the 3D-printed slab, (c) top view of the dosimeter placed inside the phantom, (d) schematic diagram of the low-cost dosimeter positioned at 10 cm depth. 3D: Three-dimensional
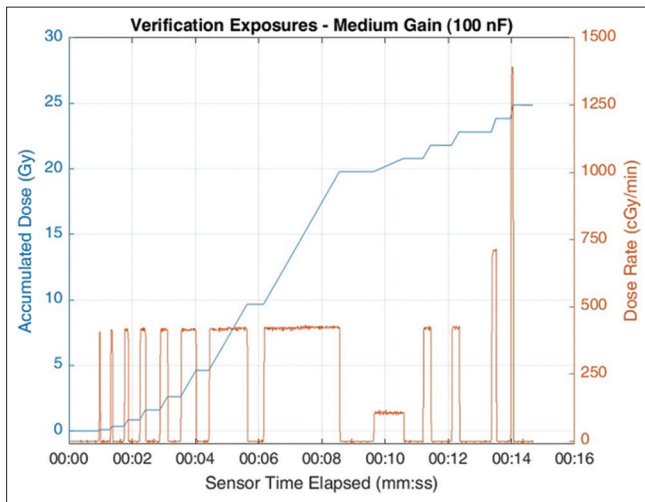

Figure 5: Cumulative plot of gain linearity verification and dose rate dependence verification exposures using a 6 MV 400 MU/min beam at 100 samples/sec

Table 1: Comparison between administered and measured dose demonstrating dose linearity (10×10 cm² field size; 90 cm SSD, 10 cm depth: 1 cGy/monitor units)

Delivered MU	Measured dose (Gy)	
	Mean (Gy)	Resolution
10	0.0989±0.0010	0.0011 Gy
25	0.252±0.0020	
50	0.502±0.0039	
75	0.756±0.0057	
100	1.006±0.0053	
200	2.007±0.0051	
500	5.026±0.0064	
1000	10.064±0.0063	

MU: Monitor units, SSD: Source to surface distance

Table 2: Orientation sensitivity dependence table of S5MC-13-F

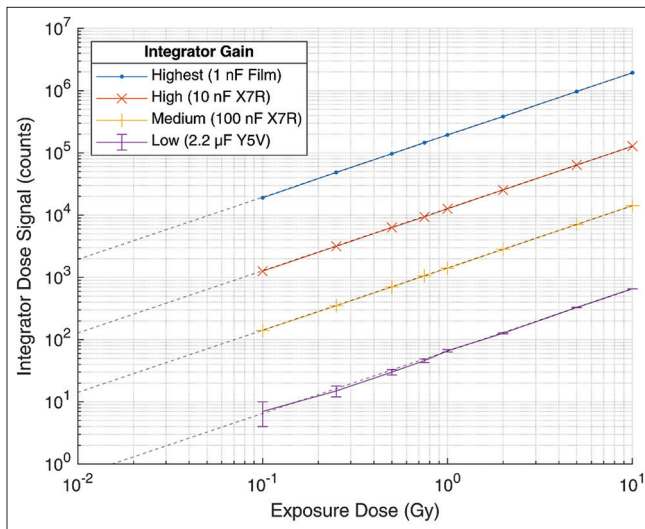| Orientation	Gantry angle (°)	Delivered (Gy)	Measured (Gy)
Top up	0	1	1.004±0.005
Bottom up	90	1	0.992±0.006
Anode up	180	1	1.10±0.003
Cathode up	270	1	1.073±004

Figure 6: Gain linearity verification results for 6 MV 400 MU/min beam at 100 samples/sec

measurements. As a result, the current design is confined to utilization at gantry angles of 0° and 180°.

The integration of the CSA front-end using a combination of precision operational amplifiers, analog switches, and precision film capacitors further enhances the precision and sensitivity of the dosimeter. Some electronic components in this simple design such as the CSA will be exposed to radiation during routine use of this detector, leading to the risk of changes in detector response and component failure with cumulative dose. This risk can be mitigated by implementing a quality assurance program that involves routine detector constancy checks, which are not dissimilar to procedures used for commercially available detectors.[18] For example, the detector could be cross-checked against an ionization chamber used for monthly dose outputs.

The selection of the S5MC-13F power diode as the radiation-sensitive detector is notable for its cost-effectiveness,

potentially making the dosimeter solution accessible to a broader range of users. The promising results observed with dose linearity, dose rate dependence, and field size dependence provide an assessment of the dosimeter's reliability under conditions for routine dosimetric quality assurance. The minimal observed average dose differences between delivered and measured doses encourage the use of the dosimeter for absolute dose measurements.

This low-cost architecture is being adapted further for a scalable, cost-effective solution for stereotactic radiotherapy/radiosurgery dosimetry, aiming to acquire signals from 120 diodes. This enhancement involves a FPGA (Field Programmable Gate Array) based integrator utilizing an adjustable discrete charge comparator front-end which removes the costly requirement for an ADC for each diode while facilitating simultaneous measurements at up to 100 samples/sec across all diodes, albeit at a slightly reduced resolution.

The low-cost dosimeter has demonstrated good performance, providing excellent dose rate and dose resolution. This makes it practical for analyzing the performance of radiation sources and deriving reliable dosimetry results. Such an affordable option could be invaluable for clinics with limited resources, serving as an integral component of a cost-effective, comprehensive quality assurance system for dosimetry in clinical settings. It is well suited for daily quality assurance of clinical linear accelerators, facilitating a rapid assessment of absolute dose.[19] The dosimetric performance of the detector indicates that this could also be used for other routine relative dosimetry applications using a solid phantom, such as measurements of linac dose rate dependence, dose linearity, field size dependence, and other measurements performed at a gantry angle of 0°.

Financial support and sponsorship

Conflicts of interest

There are no conflicts of interest.

References

1. Delaney G, Jacob S, Featherstone C, Barton M. The role of radiotherapy in cancer treatment: Estimating optimal utilization from a review of evidence-based clinical guidelines. Cancer 2005;104:1129-37.
2. Darafsheh A, editor. Radiation Therapy Dosimetry: A Practical Handbook. Boca Raton: CRC Press; 2021.
3. Ravichandran R, Binukumar JP, Davis CA. Estimation of absorbed dose in clinical radiotherapy linear accelerator beams: Effect of ion chamber calibration and long-term stability. J Med Phys 2013;38:205-9.
4. Burns JE. Absorbed-dose calibrations in high-energy photon beams at the National Physical Laboratory: Conversion procedure. Phys Med Biol 1994;39:1555-75.
5. Kumar R, Sharma SD, Philomina A, Topkar A. Dosimetric characteristics of a PIN diode for radiotherapy application. Technol Cancer Res Treat 2014;13:361-7.
6. Podgorsak EB. Radiation Oncology Physics. IAEA, Vienna; 2005.
7. Laub WU, Crilly R. Clinical radiation therapy measurements with a new commercial synthetic single crystal diamond detector. J Appl Clin Med Phys 2014;15:4890.
8. Ramachandran P, Smith A, Hagekyriakou J, Hughes J, Lonski P, Howard B, et al. Contralateral breast dose with electronic compensators and conventional tangential fields – A clinical dosimetric study. Z Med Phys 2021;31:347-54.
9. Broadhead B, Noble C, Ramachandran P. A direct comparison of the optically stimulated luminescent properties of BeO and Al (2) O (3) for clinical in-vivo dosimetry. Phys Eng Sci Med 2022;45:859-66.
10. Prabhakar R, Julka PK, Malik M, Ganesh T, Joshi RC, Sridhar PS, et al. Comparison of contralateral breast dose for various tangential field techniques in clinical radiotherapy. Technol Cancer Res Treat 2007;6:135-8.
11. Esen N, Ramachandran P, Geso M. SABR pre-treatment checks using alanine and nanoDot dosimeters. J Radiat Res 2021:rrab056.
12. Ramachandran P, Tajaldeen A, Taylor D, Wanigaratne D, Roozen K, Geso M. Evaluation and performance of ArcCheck and film using gamma criteria in pre-treatment quality assurance of stereotactic ablative radiotherapy. J Med Phys 2017;42:251-7.
13. Wen N, Lu S, Kim J, Qin Y, Huang Y, Zhao B, et al. Precise film dosimetry for stereotactic radiosurgery and stereotactic body radiotherapy quality assurance using Gafchromic™ EBT3 films. Radiat Oncol 2016;11:132.
14. Olding T, Holmes O, Dejean P, McAuley KB, Nkongchu K, Santyr G, et al. Small field dose delivery evaluations using cone beam optical computed tomography-based polymer gel dosimetry. J Med Phys 2011;36:3-14.
15. Jacqmin DJ, Miller JR, Barraclough BA, Labby ZE. Commissioning an Exradin W2 plastic scintillation detector for clinical use in small radiation fields. J Appl Clin Med Phys 2022;23:e13728.
16. Baskar R, Itahana K. Radiation therapy and cancer control in developing countries: Can we save more lives?. Int J Med Sci 2017;14:13-7.
17. Yorke AA, Williams VM, Elmore S, Alleyne-Mike K, Addison E, Jnr PO, Tagoe SN, et al. Radiotherapy physics quality assurance and management practices in low-and middle-income countries: An initial pilot survey in six countries and validation through a site visit. Adv Radiat Oncol 2023:101335.
18. Patel I, Weston S, Palmer A. IPEM report 81. Physics Aspects of Quality Control in Radiotherapy. 2nd ed. IOP Publishing Ltd: Institution of Physics Engineering in Medicine and Biology; 2018.
19. Smith K, Balter P, Duhon J, White GA Jr, Vassy DL Jr, Miller RA, et al. AAPM medical physics practice guideline 8.a.: Linear accelerator performance tests. J Appl Clin Med Phys 2017;18:23-39.